

Hybrid photonic crystal light-emitting diode renders 123% color conversion effective quantum yield

C. KRISHNAN,¹ M. BROSSARD,^{2,5,*} K.-Y. LEE,³ J.-K. HUANG,³ C.-H. LIN,^{3,4} H.-C. KUO,⁴
M. D. B. CHARLTON,¹ AND P. G. LAGOUDAKIS²

¹School of Electronics and Computer Science, University of Southampton, SO17 1BJ Southampton, UK

²School of Physics and Astronomy, University of Southampton, SO17 1BJ Southampton, UK

³Luxtaltek Corporation, Chunan Miaoli 350, Taiwan

⁴Department of Photonics & Institute of Electro-Optical Engineering, National Chiao Tung University, Hsinchu 300, Taiwan

⁵Center for Photonics and Quantum Materials, Skolkovo Institute of Science and Technology, Moscow 143026 Russia

*Corresponding author: m.brossard@soton.ac.uk

Received 16 December 2015; revised 20 February 2016; accepted 20 February 2016 (Doc. ID 255792); published 10 May 2016

Colloidal quantum dots (QDs) have emerged as promising color conversion light emitters for solid-state lighting applications [Nat. Photonics 7, 13 (2012)] due to their emission tunability and near-unity photoluminescence quantum yields. In the current commercial LEDs, QDs are dispersed into an encapsulation layer in a far-field architecture, where the majority of the light emitted by the LED remains trapped within the epitaxy due to total internal reflection, drastically reducing the out-coupling efficiency. In this paper, we demonstrate a photonic quasi-crystal hybrid LED geometry that allows QD emitters to be placed in close proximity to the multiple quantum wells (MQWs) of the active area. This architecture greatly improves the coupling between MQWs and QDs, simultaneously allowing for a non-radiative resonant energy transfer between the MQWs and the QDs and near-field radiative coupling of trapped (guided) modes in the LED to the emitters. In this configuration, we demonstrate record-breaking effective quantum yields reaching 123% for single-color conversion LEDs and 110% for white light-emitting devices.

Published by The Optical Society under the terms of the [Creative Commons Attribution 4.0 License](https://creativecommons.org/licenses/by/4.0/). Further distribution of this work must maintain attribution to the author(s) and the published article's title, journal citation, and DOI.

OCIS codes: (250.5590) Quantum-well, -wire and -dot devices; (230.5298) Photonic crystals; (230.3670) Light-emitting diodes; (260.2160) Energy transfer.

<http://dx.doi.org/10.1364/OPTICA.3.000503>

1. INTRODUCTION

With the advent of near-unity photoluminescence quantum yields (PL-QYs) [1,2] and the promise of controllable narrow emission bands, quantum dots (QDs) have been heralded in recent years as potentially groundbreaking emitting materials for color conversion applications [3]. While the direct utilization of QDs as electrically excited emitters is an inspiring prospect, the reported external quantum efficiencies of such devices remain low, with values around 20% [4,5], compared to 30–40% [6] for typical III-V devices. The incorporation of QDs as color converters in traditional solid-state devices has proven more successful, QD LED displays being an especially striking example [7]. In these devices, QDs are typically dispersed into a polymer film on the surface of the LED chip. In this far-field configuration, only photons escaping from the LED stack can be absorbed by the emitters. Most of the blue light emitted within the LED gets trapped in its epitaxial layers due to total internal reflection, resulting in poor radiative coupling between the blue light field of the MQWs and the QDs. This

dramatically reduces the overall efficiency of such white LED architectures. A common approach to improve the coupling efficiency between the LED and QDs is to roughen the LED surface or to etch nanostructures into the LED surface in the form of photonic crystals. These etched structures only typically penetrate the top barrier layer and act as diffraction gratings [8,9], enhancing the extraction efficiency of the MQW emission. While nanohole [10] or nanorod [11] structures penetrating the active area were shown to improve the color conversion efficiency, poor sidewall quality and overly simple photonic crystal designs have so far limited the performance of such devices.

In this paper, we present an efficient hybrid 12-fold photonic quasi-crystal (PQC) multi-quantum well (MQW) white LED geometry that allows a drastic improvement of the out-coupling efficiency while retaining the good electrical properties of the unpatterned devices. We demonstrate that this architecture allows electrically injected carriers to efficiently couple to the QDs through nonradiative resonant energy transfer while allowing near-field coupling between the blue light field and the emitters

within the LED. This results in record-breaking effective quantum yields reaching 123% for single-color QDs and 110% for white LEDs.

2. DEVICE CHARACTERIZATION

A. Sample Description

The devices studied in this paper consist of GaN/InGaN MQW LEDs on patterned sapphire substrates into which 12-fold symmetric quasi-crystals (PQCs) were fabricated using low-cost nano-imprint lithography and plasma etching [see Fig. 1(a) and the Methods section]. As can be seen in the cross-sectional scanning electron microscope (SEM) image in Fig. 1(b), the PQC structure penetrates through the MQW active area, forming an array of 480 nm radius cylindrical holes with a lattice pitch of 750 nm. A top SEM image of the etched structure is provided in Fig. 1(c). This high-symmetry PQC exhibits long-range order and short-range disorder and possesses semi-random properties. This geometry has been shown to be far superior to the regular photonic crystal lattices commonly adopted for LED applications, due to its highly symmetrical far-field beam shape, and to the relative increase in the density of states, which greatly increases light extraction [12,13]. The PQCs were integrated into modular LED chips using photolithography and wet and dry etching techniques. Etching an LED induces shunt paths and creates non-radiative recombination centers through dangling bonds on the sidewalls. Here, we have alleviated such detrimental effects by refining the etching process to create smooth sidewalls and by passivating the etched devices using thermal annealing at 500°C in a nitrogen atmosphere. The latter dramatically improves the electrical properties of the etched LEDs.

Three different “off-the-shelf,” nearly monodispersed $\text{CdS}_x\text{Se}_{1-x}/\text{ZnS}$ core/shell colloidal semiconductor QDs emitting at 535, 585, and 630 nm (herein QD-535, QD-585, and QD-630) were chosen as the color converters. Spin coating was used to hybridize the PQC LEDs with QD emitters. The spin-coating parameters were tuned so as to completely fill the nanohole

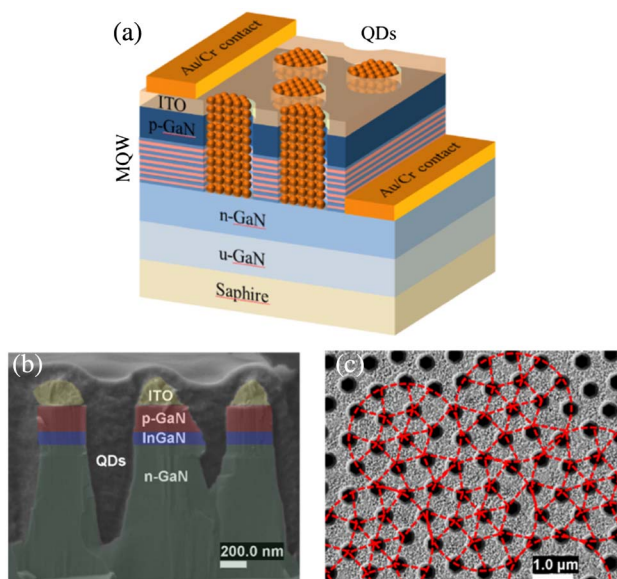


Fig. 1. (a) Schematic representation, (b) cross-sectional, and (c) top SEM images of a photonic quasi-crystal LED hybridized with QD color converters.

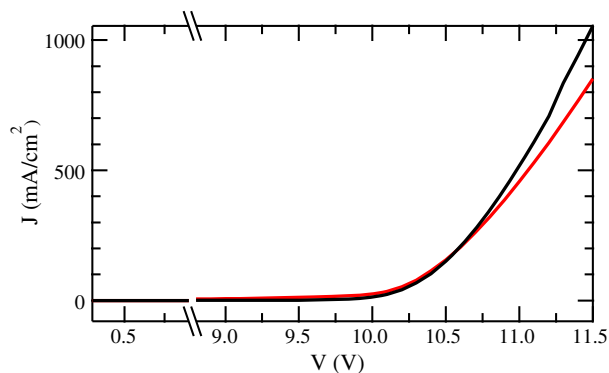


Fig. 2. J–V characteristics of a planar (black solid line) and of a PQC (red solid line) LED.

cavities with emitters, as shown in Fig. 1(b). Hybridization with QDs was found to weakly impact the electrical properties (see Supplement 1). PQC LEDs were hybridized with both single-color QDs and with a cocktail of three different colored QDs to obtain single-color conversion and white devices, respectively. In the case of the white device, the relative ratios between the three different colored QDs were tuned so as to obtain a white light spectrum close to the daylight D-65 standard when combined with a blue LED.

B. Electrical Properties

The high-voltage LED devices used in this study incorporate four parallel arrays of twenty sub-LEDs connected in series on the same chip. By increasing the operation voltage and thus decreasing the driving currents for a given input power, these devices can drastically limit the efficiency droop occurring at high driving currents. Using a higher operation voltage also allows simpler power transformer designs and can improve device reliability. The electrical properties of the LED chips were studied with and without the PQC. The J–V characteristics are presented in Fig. 2 for a planar device (red solid line) and for a PQC device (black solid line). The current density of the PQC structure is found to be slightly higher than the planar case at a low voltage, indicating the presence of minor shunting paths in the PQC sidewalls. Etching the PQC structure weakly lowers the current density at higher voltages, with a maximum relative drop of ~19% at 11.5 V. The increase of the series resistance in the PQC case is attributed to the relatively poorer current-spreading properties in the top layers after etching. Importantly, the turn-on voltage is found in both cases to be ~10.3 V. These results, which are very similar to the best reported values in the literature [14,15], indicate a very good nanohole sidewall quality.

3. ELECTROLUMINESCENCE SPECTRA

A single-color conversion device was hybridized with QDs emitting at 585 nm. Figure 3(a) shows the electroluminescence (EL) spectra before (black solid line) and after (red solid line) hybridization along with the absorption spectrum of the QDs (orange dashed line). White-light LEDs were fabricated using a blend of green, orange, and red emitters (QD-535, QD-585, and QD-630). Figure 3(b) shows the EL spectrum of the PQC LED before (black solid line) and after (red solid line) hybridization with the QD blend along with the absorption spectra

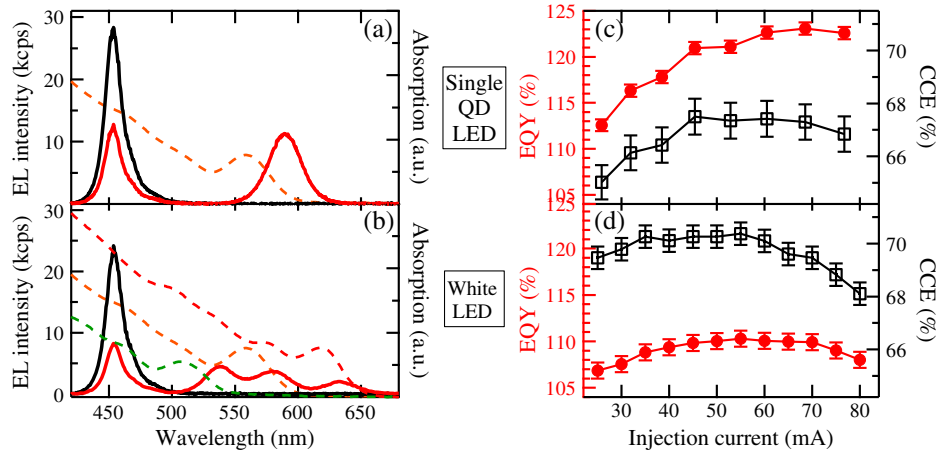


Fig. 3. (a, b) Electroluminescence spectra of a PQC LED before (black solid line) and after hybridization (red solid line) with (a) QD-585 and (b) a blend of QD-535, QD-585, and QD-630, along with the absorption spectrum of QD-585 (orange dashed line) in (a) and the absorption spectrum of QD-535 (green dashed line), QD-585 (orange dashed line), and QD-630 (red dashed line) in (b). (c, d) Effective quantum yield (red solid circles) and effective color conversion efficiency (black open squares) of a PQC LED hybridized with QD-585 in (c) and with the QD blend in (d). The solid lines are a guide for the eye.

of the different QD colors (green, orange, and red dashed lines). We note the strong spectral overlap between the absorption of the various QDs and the LED EL, a prerequisite for efficient energy transfer between the MQWs and the QD emitters. The relatively narrow (~ 30 nm FWHM) QD luminescence maxima observable in the hybrid EL spectra are in good agreement with the PL properties of the QDs on glass (see Supplement 1). In both the single-color QD and blended QD cases, the EL maximum of the LED is found to be strongly quenched by the presence of the QDs, indicating the presence of a significant energy transfer from the MQW to the QDs.

A. Color Conversion Efficiency

The overall amount of energy transfer from the MQWs to the QDs, including both radiative pumping and non-radiative resonant energy transfer (RET), can be gauged using the color conversion efficiency (CCE), which is defined as the ratio of the integrated luminescence intensity of the QDs in the hybridized structure to the integrated luminescence intensity of the MQWs in the bare device [11]:

$$\text{CCE} = \frac{\int I_{\text{QDs}}^{\text{Hybrid}}(\lambda) d\lambda}{\int I_{\text{MQW}}^{\text{Bare}}(\lambda) d\lambda}, \quad (1)$$

where λ is the wavelength of light, X in I_X^Y denotes the EL intensity of the QDs or MQWs, and Y denotes the bare or hybrid structures. Further on, we estimate the effective quantum yield (EQY) of the color conversion process, which is defined as the ratio of the number of emitted photons at the QD wavelength to the number of photons effectively quenched at the emission wavelength of the MQWs after hybridization:

$$\text{EQY} = \frac{\int I_{\text{QDs}}^{\text{Hybrid}}(\lambda) d\lambda}{\int I_{\text{MQW}}^{\text{Bare}}(\lambda) d\lambda - \int I_{\text{MQW}}^{\text{Hybrid}}(\lambda) d\lambda}. \quad (2)$$

It is important to note that in the definition of the EQY, the denominator is given by the difference in the intensity of the MQWs before and after hybridization. Some of this quenching is due to QD absorption; however, depositing the QDs also

modifies the out-coupling efficiency [13] of the MQW emission. This is especially the case for etched PQC, for which the out-coupling efficiency strongly depends on the refractive index contrast between the epitaxy and the material filling the nanoholes. These effects explain the high values reported in the literature [16,17] (typically higher than the PL-QY of the QDs) and indeed, the results presented in this paper. While this definition can lead to EQYs in excess of 100%, no multi-photon processes are involved.

Figure 3(c) shows both CCE and EQY of the QD-585 hybridized PQC LED as a function of the injection current. With increasing driving currents, the CCE is found to slightly increase and then remain virtually constant, with an average of 66.7% and a standard deviation of 0.8%. These values, which are much higher than the CCEs reported in [11,18–20], are a strong indicator that the QDs efficiently couple to guided modes in the LED. The EQY of the QDs is found, on the other hand, to be significantly dependent on the injection current, with a gradual 9% relative increase from 25 mA to its maximum value of 123% at ~ 70 mA. It is conceivable that the initial EQY increase is related to the thermal activation of trapped carriers in the QDs [17], which would increase their PL-QY. The decrease above 70 mA is attributed to a temperature quenching of the PL-QY of the QDs, which was previously reported in the literature for such emitters [21]. The 123% maximum EQY value represents a large 30% relative increase compared to the previous best reported values ($\sim 95\%$ in [16,17]). It is also important to note that this result was obtained with standard off-the-shelf QDs with $\sim 40\%$ PL-QY (see [22]). Since the PL-QY of the QDs remains a bottleneck for all color conversion processes, using state-of-the-art emitters providing PL-QYs in excess of 80% [1,2] could potentially double the EQY of our devices and drastically improve LED performance.

The CCE and the EQY of the device hybridized with the QD blend are plotted in Fig. 3(d) as a function of the injection current. As in the previous case, both values are found to gradually increase with the increasing current before reaching their maxima at approximately 60 mA and dropping for higher currents. The

CCE is found to be similar to the single-color case, with values ranging from 68% to 70%. This is a good indication that the overall QD density is similar for both blended and single-color QD hybridized devices, which is in good agreement with SEM cross-sectional studies indicating fully filled nanoholes [see Fig. 1(c) and Supplement 1]. The EQY of the white device is found, on the other hand, to be significantly decreased compared to the single-color QD case, with a maximum value of $\sim 110\%$. This $\sim 10\%$ relative decrease from the single-color QDs to the blend is attributed to energy transfers, both radiative and non-radiative, between the three different colors within the blend. Using state-of-the-art QDs with PL-QYs in excess of 80% would alleviate this mismatch to a significant extent.

B. CIE Coordinates

The CIE (Commission Internationale de l'Éclairage) coordinates of the various hybrid PQC LEDs reported in this paper were calculated using their EL spectra and are displayed in Fig. 4 for an injection current of 80 mA. The white LED device was found to be at (0.312, 0.337) in the CIE map (red star), and its correlated color temperature (CCT) was calculated to be 6509 K. These coordinates are a good match to the 6500 K D65 daylight standard at (0.313, 0.329). Both the CCT and CIE coordinates are found to remain stable for a range of injection currents (20–85 mA), with small relative variations of $\sim 5\%$ across the current range (see Supplement 1). The CIE of the PQC LED hybridized with QD-585 was found to be (0.3861, 0.2668) and is annotated in Fig. 4 by a green circle. These coordinates were also found to be weakly dependent on the injection currents between 20 and 80 mA. By tuning the ratio of the various components of the tri-color QD blend, the CCT could be tuned between 12,928 and 6509 K (black stars in Fig. 4).

4. TIME-RESOLVED SPECTROSCOPY

Time-resolved photoluminescence (TRPL) spectroscopy was used to study the non-radiative resonant energy transfer between the MQWs and the QD color converters. The samples were excited at 380 nm using a frequency-doubled Ti:sapphire laser.

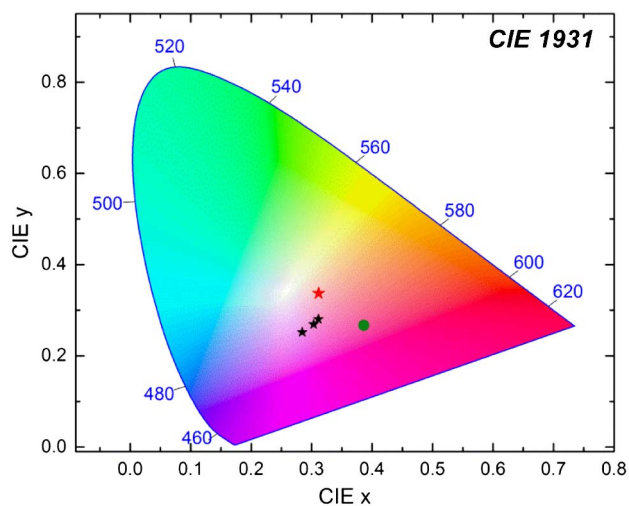


Fig. 4. Chromaticity diagram indicating the CIE coordinates for PQC LEDs hybridized with QD-585 (green circle), with the tri-color QD blend (red star) and for variations of the blend ratio (black stars). Measurements are reported for an 80 mA injection current.

The excitation density was kept constant at ~ 40 nJ/cm². The PL was detected using a fast avalanche photodiode and time-correlated single photon counting electronics (~ 50 ps temporal resolution). The PL decays of the MQW before (black continuous) and after (red continuous) hybridization with QD-585 (single-color QD device) and with the tri-color QD blend are displayed in Figs. 5(a) and 5(b), respectively. The decay dynamics are found to be strongly accelerated after hybridization, indicating the presence of an additional recombination channel in the MQWs attributed to RET. The decays were fitted with a double-stretched exponential function:

$$I(t) = Ae^{-(k_r + k_{\text{RET}})t} + Be^{-(k_r)^\beta t}, \quad (3)$$

where $I(t)$ is the time-dependent PL intensity, and k_r and k_{RET} are the recombination (radiative and other non-radiative channels) and RET decay rates, respectively. β is a stretched exponent, A denotes the fraction of excitons close enough to the MQW sidewalls to undergo RET, and B is the fraction of excitons that do not contribute to RET. The sum of A and B is kept constant and equal to one. In this equation, the stretched exponentials account for the presence of a distribution of other non-radiative decay channels induced by residual defects and dangling bonds on the PQC sidewalls. Thus, β can loosely represent a quality factor for the distribution of decay rates, with $\beta = 1$ corresponding to devices with single k_r and k_{RET} rates.

In the single-color QD case, the bare decay was fitted by setting k_{RET} to zero, which yielded a recombination lifetime of 3.2 ns and a β value of 0.82. The high value of β indicates the high quality of the nanohole sidewalls passivation and is in good agreement with the good electrical properties presented previously. The recombination and RET lifetimes were extracted by fitting the decay of the hybrid device, keeping $\beta = 0.82$, which yielded recombination and RET lifetimes of 3.3 and 0.57 ns, respectively. The excellent agreement between the recombination lifetimes of the hybrid and bare devices indicates that hybridization does not impact the exciton recombination dynamics of

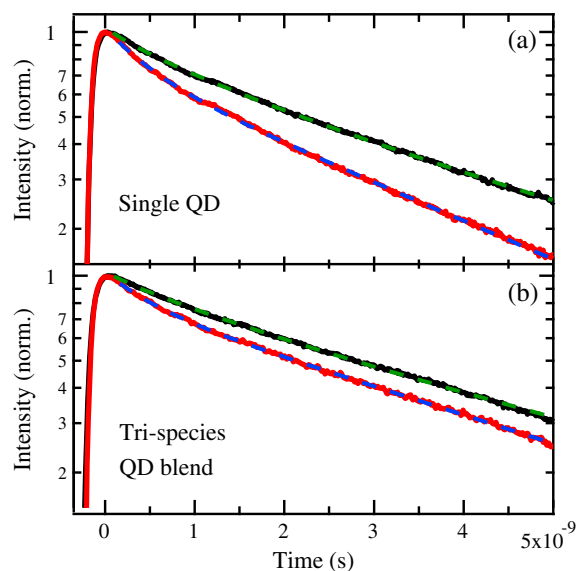


Fig. 5. Time-resolved photoluminescence decays of a PQC LED before (black) and after (red) hybridization with QD-585 in (a) and with the tri-color QD blend in (b). The dashed lines indicate best fits to the experimental data using Eq. (3).

the MQWs. This allows us to conclude that hybridizing with QDs does not affect or create surface recombination channels at the MQW/QD interface. Nearly a quarter, 23%, of the MQW exciton population is found to participate in RET. The RET efficiency η_{RET} , defined as $\eta_{\text{RET}} = \frac{k_{\text{RET}}}{k_{\text{RET}} + k_r}$, is calculated to be 85%, in good agreement with previous reports [20,22]. From these numbers, we can estimate that $A * \eta_{\text{RET}} \simeq 20\%$ of the excitons in the MQW transfer non-radiatively to the QD emitters.

A similar analysis was carried out on the white light device. Fitting the PL decay of the bare structure yielded a recombination lifetime of 4.3 ns and a stretching factor β of 0.89. The higher β value compared to the single QD case indicates an improved sidewall surface quality (attributed to sample-to-sample variations), which results in a higher exciton recombination lifetime. A best fit of the PL decay of the structure hybridized with the tri-species blend (β kept constant and equal to 0.89) provided recombination and RET lifetimes of 4.5 and 0.92 ns, respectively. The fraction of MQW excitons undergoing RET was found to be 22%, similarly to the single QD case. Calculating the RET efficiency yielded a value of 80%, in good agreement with the single QD species case and the literature.

5. DISCUSSION AND CONCLUSION

In a typical flat GaN LED grown on a sapphire wafer, only $\sim 6\%$ of the light is extracted toward the top transparent contact, while about 60% to 80% [12,23] of the light is trapped within the GaN slab by total internal reflection at the GaN/air and GaN/sapphire interfaces, depending on the LED configuration. About half of these photons are waveguided into higher-order modes and are potentially extractable using photonic crystal diffraction gratings or plasmonic structures, while the other half is guided into low-order modes and remains mostly confined within the GaN [23]. The evanescent field of these guided modes can extend up to 100 nm in the nanoholes for visible wavelengths [24]. By etching nanoholes into the MQW area, we allow our emitters to non-radiatively couple into both higher- and lower-order modes. The presence of this additional population of excitation photons strongly enhances the overall absorption of the QDs. This reasoning is especially true for PQC compared to lower-symmetry photonic crystals (PhCs). Indeed, the high symmetry of the PQCs and the size of their Brillouin zones allow the presence of large higher energy bands, while in PhCs, only a few modes are present. The modes making up this band can efficiently “leak” into the nanoholes, where they are scattered out. In our hybrid structure, these modes can efficiently couple to the QD emitters. This effect, combined with the high 20% non-radiative energy transfer probability from the MQW to the QDs, can explain the very large effective EQYs and CCEs reported herein.

In conclusion, we demonstrated a high-performance hybrid QD PQC LED geometry that provides record color conversion performance. This is made possible by combining a high-symmetry PQC geometry that provides high out-coupling efficiencies with good sidewall treatment, allowing us to etch through the MQW active area without significantly damaging the electrical properties. This architecture allows us to place QD emitters in close proximity to the MQWs, which enables the non-radiative pumping of the emitters by the MQW, and within the GaN slab, which allows the QDs to couple to lower-order guided modes within the epitaxy. We report effective quantum yields for the QD emitters reaching 123% for single QD species color

converters, and slightly lower values of $\sim 110\%$ for the a tri-species white QD blend. These results surpass previous reports by more than 30%. We utilize this approach to fabricate a hybrid white LED with a record color conversion performance and a quasi-perfect 6500 K D65 spectrum. The performances of these hybrid devices, using “off-the-shelf” QDs, could be strongly improved by utilizing state-of-the-art nanocrystalline emitters, potentially doubling the color conversion effective quantum yield. We believe that these hybrid PQC LED structures, fabricated with low-cost nano-imprint lithography and using cheap colloidal QD emitters, could represent an important technological breakthrough for the solid-state lighting industry. By effectively integrating the color conversion emitters into the epitaxy, these white LED chips could, for instance, be incorporated into the edge-lighting strips of LED-backlit LCD displays. This approach would remove the need for a color conversion layer under the LCD stack and simplify the assembly of QD color conversion displays, significantly lowering manufacturing costs.

6. METHODS

A. Fabrication

The LED epi-structure was grown on a patterned sapphire substrate via metal organic chemical vapor deposition using a bottom-to-top approach, which involved sequentially depositing a 50 nm GaN nucleation layer, a 2 μm un-doped GaN buffer layer, a 3 μm Si-doped n-GaN layer, ten pairs of $\text{In}_{0.21}\text{Ga}_{0.79}\text{N}/\text{GaN}$ MQWs with a central wavelength of 453 nm, and a 200 nm Mg-doped p-GaN layer. After the growth of the LED wafer, a 230 nm indium tin oxide (ITO) transparent conducting layer was e-beam evaporated on the top of the LED wafer. Nano-imprint lithography (NIL) and photolithography were used to define nanoholes within a selected mesa area. A 400-nm-thick SiO_2 layer was first deposited on the surface of the prepared LED wafer by plasma-enhanced chemical vapor deposition and a 360-nm-thick imprint-resist (IR) layer was spin coated onto the SiO_2 layer at 3000 rpm. By placing and releasing a nano-imprint mold on the IR layer, a 12-fold photonic quasi-periodic crystal nanohole pattern was transferred to the IR layer. SiO_2 nanoholes were formed through a two-step plasma reactive ion etching (RIE) technique using O_2 and CHF_3 process gases. A photoresist (PR) layer was deposited onto the SiO_2 layer and patterned using standard photolithography to define selected dry-etching areas. The LED wafer with a PR layer and a nano-patterned dielectric layer was etched in an inductively coupled plasma reactive ion etching (ICP-RIE) system with mixed process gases of Cl_2 and BCl_3 ($\text{Cl}_2/\text{BCl}_3 = 20/10$ sccm) at a bias power of 100 W and an ICP power of 100 W.

To complete the modular array LED chip, the PQC LED wafer was taken through a link-chip process. The patterning of the ITO and of the mesa layer was done using a standard chip process utilizing photolithography and wet- and dry-etching steps. The ITO thin film on the LED wafer was etched to form an ohmic-contact layer in a wet etching system using a mixed HCl/FeCl_3 solution after pattern definition using photolithography. The mesa area was then defined by photolithography and mesa etching was performed with $\text{Cl}_2/\text{BCl}_3/\text{Ar}$ etching gas in an ICP-RIE system, which transferred the mesa pattern onto the n-GaN layer. To obtain chip isolation, a PR/ SiO_2 (2 $\mu\text{m}/$ 1 μm) layer was employed as an etching mask in a slow dry

etch. The sidewalls of isolated chips were then passivated with a 0.5 μm SiO_2 dielectric film. A multi-metal layer ($\text{Cr}/\text{Au} = 50/1500$ nm) was formed onto the surface of the ITO and of the n-GaN via e-gun evaporation system and PR liftoff. The final LED structure consisted of 80 link chips ($1.1 \text{ mm} \times 0.2 \text{ mm}$) integrated into a 25 mm^2 chip area.

The QDs used for device hybridization were Trilite fluorescent nanocrystals procured from Cytodiagnosics. These $\text{CdS}_x\text{Se}_{1-x}/\text{ZnS}$ core/shell colloidal semiconductor QDs (oleic acid capped, dispersed in toluene) were found to have 1 s emission peaks at 535 ± 15 nm (herein QD-535), 535 ± 15 nm (QD-585), and 630 ± 16 nm (QD-630), and 1 s absorption peaks at 515, 560, and 620 nm, respectively. QD layers were deposited onto the PQC devices using dynamic spin coating at 1500 rpm. The EL data presented in Fig. 3 was obtained for 8.7:1 and 0.3:1 mass ratios of QD-535 to QD-585 and QD-630 to QD-585, respectively. The devices were fully characterized before and after QD hybridization.

B. Characterization Methods

J–V characterization was performed using a Keithley 2400 current-voltage unit. The LED spectra and intensities were measured inside a six-inch integration sphere coupled to a TE-cooled BWtek spectrometer. The SEM characterization of the LED and QD thickness was done using a Zeiss Nvision 40 FIB-SEM system. The absorption spectra of the QDs on glass were measured using a Jasco UV/VIS/NIR spectrophotometer.

Time-resolved photoluminescence decays were acquired using a single-photon avalanche photodiode (Micro photon devices PDM series) coupled to a Becker and Hickl SPC-140 TCSPC (time-correlated single-photon counting) acquisition card. The InGaN QWs of the LED were pumped at 380 nm using a frequency-doubled tunable femtosecond Ti:Sapphire laser (Coherent Chameleon). The excitation power was kept constant at 0.255 mW and was focused onto the sample using a $10 \times$ Nikon objective (NA = 0.50). The photoluminescence from the QWs was collected through the same objective and was filtered using a 405 nm longpass (Semrock BLP01-405R-25) and a 447 nm bandpass (Edmund optics 84-111) filter and focused onto the avalanche photo diode using a $40 \times$ Nikon objective (NA = 0.25).

Funding. Royal Society; Engineering and Physical Sciences Research Council (EPSRC) (EP/J017361/1, EP/M025330/1); UK-India Education and Research Initiative (UKIERI) (RP011266); Ministry of Science and Technology of the People's Republic of China (MOST) (MOST 104-3113-E-009-002-CC2).

Acknowledgment. M. B. and P. G. L. acknowledge support by the Engineering and Physical Sciences Research Council of the UK through the “Hybrid Polaritonics” Program Grant (Project EP/M025330/1) and through the “Supersolar Solar Energy Hub” (Project EP/J017361/1) and by the UK-India Education Research Initiative through grant RP011266. C. K. and M. D. B. C. acknowledge support by the Royal Society International Exchange Scheme. C.-H. L. acknowledges support from the Ministry of Science and Technology of the People's Republic of China, through the MOST 104-3113-E-009-002-CC2 grant. All data supporting this study are openly

available from the University of Southampton repository at <http://dx.doi.org/10.5258/SOTON/387964>.

See [Supplement 1](#) for supporting content.

REFERENCES

1. R. C. Page, D. Espinobarro-Velazquez, M. Leontiadou, C. Smith, E. Lewis, S. J. Haigh, C. Li, H. Radtke, A. Pengpad, F. Bondino, E. Magnano, I. Pis, W. R. Flavell, P. O'Brien, and D. J. Binks, “Near-unity quantum yields from chloride treated CdTe colloidal quantum dots,” *Small* **11**, 1548–1554 (2015).
2. A. B. Greytak, P. M. Allen, W. Liu, J. Zhao, E. R. Young, Z. Popović, B. Walker, D. G. Nocera, and M. G. Bawendi, “Alternating layer addition approach to CdSe/CdS core/shell quantum dots with near-unity quantum yield and high on-time fractions,” *Chem. Sci.* **3**, 2028–2034 (2012).
3. Y. Shirasaki, G. J. Supran, M. G. Bawendi, and V. Bulović, “Emergence of colloidal quantum-dot light-emitting technologies,” *Nat. Photonics* **7**, 13–23 (2012).
4. X. Dai, Z. Zhang, Y. Jin, Y. Niu, H. Cao, X. Liang, L. Chen, J. Wang, and X. Peng, “Solution-processed, high-performance light-emitting diodes based on quantum dots,” *Nature* **515**, 96–99 (2014).
5. B. S. Mashford, M. Stevenson, Z. Popovic, C. Hamilton, Z. Zhou, C. Breen, J. Steckel, V. Bulovic, M. Bawendi, S. Coe-Sullivan, and P. T. Kazlas, “High-efficiency quantum-dot light-emitting devices with enhanced charge injection,” *Nat. Photonics* **7**, 407–412 (2013).
6. Y.-R. Wu, Q. Yan, S. P. DenBaars, C. Van de Walle, H. Fu, S. Nakamura, Y. Zhao, and C.-C. Pan, “High optical power and low-efficiency droop blue light-emitting diodes using compositionally step-graded InGaN barrier,” *Electron. Lett.* **51**, 1187–1189 (2015).
7. MMD and QD Vision, *MMD, QD Vision Introduce World's First Quantum Dot Monitor* (2015).
8. J. J. Wierer, A. David, and M. M. Megens, “III-nitride photonic-crystal light-emitting diodes with high extraction efficiency,” *Nat. Photonics* **3**, 163–169 (2009).
9. C. Wiesmann, K. Bergeneck, N. Linder, and U. T. Schwarz, “Photonic crystal LEDs—designing light extraction,” *Laser Photon. Rev.* **3**, 262–286 (2009).
10. M. D. B. Charlton, P. Lagoudakis, and S. Chanyawadee, “Optical device with non radiative energy transfer,” U.S. patent WO2010092362 A3 (October 14, 2010).
11. F. Zhang, J. Liu, G. You, C. Zhang, S. E. Mohney, M. J. Park, J. S. Kwak, Y. Wang, D. D. Koleske, and J. Xu, “Nonradiative energy transfer between colloidal quantum dot-phosphors and nanopillar nitride LEDs,” *Opt. Express* **20**, A333–A339 (2012).
12. M. D. B. Charlton, “Photonic crystal nitride LEDs,” in *Nitride Semiconductor Light-Emitting Diodes (LEDs): Materials, Technologies and Applications* (Woodhead, 2014), pp. 301–354.
13. N. Ganesh, W. Zhang, P. C. Mathias, E. Chow, J. A. N. T. Soares, V. Malyarchuk, A. D. Smith, and B. T. Cunningham, “Enhanced fluorescence emission from quantum dots on a photonic crystal surface,” *Nat. Nanotechnol.* **2**, 515–520 (2007).
14. Y. C. Shin, D. H. Kim, E. H. Kim, J. M. Park, K. M. Ho, K. Constant, J. H. Choe, Q. Han Park, H. Y. Ryu, J. H. Baek, T. Jung, and T. G. Kim, “High efficiency gan light-emitting diodes with two dimensional photonic crystal structures of deep-hole square lattices,” *IEEE J. Quantum Electron.* **46**, 116–120 (2010).
15. J. Bai, Q. Wang, and T. Wang, “Greatly enhanced performance of InGaN/GaN nanorod light emitting diodes,” *Phys. Status Solidi* **209**, 477–480 (2012).
16. V. Wood and V. Bulović, “Colloidal quantum dot light-emitting devices,” *Nano Rev.* **1**, 5202 (2010).
17. J. S. Steckel, J. Ho, C. Hamilton, C. Breen, W. Liu, P. Allen, J. Xi, and S. Coe-Sullivan, “Quantum dots: the ultimate down-conversion material for LCD displays,” *SID Symp. Dig. Tech. Pap.* **45**, 130–133 (2014).
18. M. Achermann, M. Petruska, D. D. Koleske, M. H. Crawford, and V. I. Klimov, “Nanocrystal-based light-emitting diodes utilizing high-efficiency nonradiative energy transfer for color conversion,” *Nano Lett.* **6**, 1396–1400 (2006).

19. M. J. Park, K. J. Choi, and J. S. Kwak, "Enhanced color-conversion efficiency between colloidal quantum dot-phosphors and nitride LEDs by using nano-patterned p-GaN," *J. Electroceram.* **33**, 2–6 (2014).
20. S. Chanyawadee, P. G. Lagoudakis, R. T. Harley, M. D. B. Charlton, D. V. Talapin, H. W. Huang, and C.-H. Lin, "Increased color-conversion efficiency in hybrid light-emitting diodes utilizing non-radiative energy transfer," *Adv. Mater.* **22**, 602–606 (2010).
21. Y. Zhao, C. Riemersma, F. Pietra, R. Koole, C. de Mello Donegá, and A. Meijerink, "High-temperature luminescence quenching of colloidal quantum dots," *ACS Nano* **6**, 9058–9067 (2012).
22. M. Brossard, C.-Y. Hong, M. Hung, P. Yu, M. D. B. Charlton, P. G. Savvidis, and P. G. Lagoudakis, "Novel non-radiative exciton harvesting scheme yields a 15% efficiency improvement in high-efficiency III-V solar cells," *Adv. Opt. Mater.* **3**, 263–269 (2015).
23. A. David, T. Fujii, R. Sharma, K. McGroddy, S. Nakamura, S. P. DenBaars, E. L. Hu, C. Weisbuch, and H. Benisty, "Photonic-crystal GaN light-emitting diodes with tailored guided modes distribution," *Appl. Phys. Lett.* **88**, 061124 (2006).
24. F. S. Diana, A. David, I. Meinel, R. Sharma, C. Weisbuch, S. Nakamura, and P. M. Petroff, "Photonic crystal-assisted light extraction from a colloidal quantum dot/GaN hybrid structure," *Nano Lett.* **6**, 1116–1120 (2006).